PROCEEDINGS OF SCIENCE

First measurements from charmless B decays at Belle II

Yun-Tsung Lai[*†]
Kavli IPMU
E-mail: yun-tsung.lai@ipmu.jp

We report on first measurements of branching fractions, CP-violating charge-asymmetries, and polarizations in various charmless B decays at Belle II. We use a sample of electron-positron collisions at the $\Upsilon(4S)$ resonance from the SuperKEKB collider collected in 2019-2020 and corresponding to an integrated luminosity of 34.6 fb^{-1} in 2019 and 2020. All results are consistent with world average and provide extensive validations of the detector performances and analysis strategies.

The 19th International Conference on B-Physics at Frontier Machines (BEAUTY 2020)
21-24 September, 2020
Remote conference

[*] Speaker.
[†] On behalf of the Belle II Collaboration.

1. Introduction

Charmless B decays are important to search for non-standard-model physics in the flavor sector. Many decay channels are governed by ‘penguinâĂŹ amplitudes, which are sensitive to non-Standard-Model (non-SM) contributions contributing to the loop. Studying them in detail is an important goal of the Belle II experiment. With larger amount of data, Belle II is expected to improve significantly important measurements such as the determination of the CKM phase α/ϕ_2 [1, 2], the precision test of of $K\pi$ isospin sum rule [1, 3], and the study of CP-vioalting asymmetries localized in the three-body B decays' phase space [1]. In addition, the measurement of decay-time dependent CP violation in the penguin-dominated $B^0 \to \phi K^0$ mode, compared with corresponding results from $B^0 \to J/\psi K^0$ decays, offers a sharp probe of non-SM physics. Measurements of the longitudinal polarization fractions (f_L) of decays of B mesons into pairs of vector mesons also probe non-SM dynamics. Previous measurements of f_L in $B^0 \to J/\psi K^0$ showed a sizable contribution from transverse polarization, while the logitudinal polarization is predicted to be dominant.

SuperKEKB [6] is an asymmetric e^+e^+ collider, that started the collision operations with the Belle II detector [7] from March 2019. We use a data sample of 34.6 fb^{-1}, which was collected at the Υ(4S) resonance up to May 2020. This report presents the first measurements of branching fractions ($\mathscr{B}$), CP-violating charge-asymmetries ($\mathscr{A}_{CP}$), and longitudinal polarization fractions (f_L) based on the following B decays reconstructed in Belle II data: $B^0 \to K^+\pi^-$, $B^0 \to \pi^+\pi^-$, $B^+ \to K^+\pi^0$, $B^+ \to \pi^+\pi^0$, $B^+ \to K^0\pi^+$, $B^0 \to K^0\pi^0$, $B^+ \to K^+K^-K^+$, $B^+ \to K^+\pi^-\pi^+$, $B^0 \to \phi K^0$, $B^+ \to \phi K^+$, $B^0 \to \phi K^{*0}$, and $B^{*+} \to \phi K^{*+}$ [8, 9].

The B reconstruction, event seletion scriteria, and background suppression scheme are studied with various simulated signal and background samples. Charged-particle trajectories (tracks) are identified with inner vertex detectors and central drift chamber with requirements on the displacement from the interaction point to reduce beam-background-induced tracks. The identification of charged particles uses the information from two particle-identification (PID) devices, time-of-propagation counter in the barrel region and a proximity focusing aerogel ring-image Cherenkov counter in the forward endcap region. Decays of π^0 candidates are reconstructed by using two isolated clusters in the electromagnetic calorimeter, with requirements on the helicity angle and kinematic fit to constrain π^0 mass. Decays of K_S^0 candidates are reconstructed from two opposite-charge pion candidates from a common vertex, restricted to meet additional requirements on its kinematic variables, e.g. momentum, flight distance, distance between pion trajectories, etc, to further reduce the combinatorial background. Decays of ϕ candidates are reconstructed from two opposite-charge kaon candidates. Decays of K^{*0} candidates are reconstructed from one K^+ and one π^-, and K^{*+} are reconstructed from one K_S^0 and one π^+. In three body decays, we suppress the relevant peaking backgrounds from charmed or charmonium intermediate states by excluding the corresponding two-body mass ranges.

We use the following two major variables to distinguish the signal B events from other backgrounds: the energy difference $\Delta E \equiv E_B - \sqrt{s}/2$ between the reconstrcuted B candidate and half of the collision energy in $\Upsilon(4S)$ frame, and Beam-energy-constrained mass $M_{\rm bc} \equiv \sqrt{s/(4c^2) - (p_B^*/c)^2}$.

2. Continuum background suppression

One of the main challenges of the charmless B decays' reconstruction is the large combinatorial background with the same final state from the $e^+e^- \to q\overline{q}$ $(q = u,d,s,c)$ processes. It is mainly due to rates 10^5 times smaller than continuum background and the lack of distinctive final-state features (leptons or intermediate resonances) make the reconstruction of signal hard. A binary boosted decision-tree (BDT) classifier is used to combine more than 30 variables nonlinearly. The input variables to BDT include event topology variables, flavor-tagging information, vertex-fitting information, and kinematic-fit information. All of them are required to be loosely or not correlated to ΔE and $M_{\rm bc}$.

3. Signal extraction and measurement results

We use unbinned maximum likelihood fits to extract signal yields from the data sample to calculate various physics observables. The $B \to hh$ and $B \to hhh$ ($h = K$ or π) modes use ΔE only with $M_{\rm bc} > 5.27$ GeV/c^2 in the data fit. The two $B \to \phi K$ modes use five varibles including ΔE, $M_{\rm bc}$, output of the continuum suppression BDT discriminator (C'_{out}), K^+K^- candidate mass ($m_{K^+K^-}$), and ϕ candidate's cosine of the helicity angle ($\cos\theta_{H,\phi}$). The two $B \to \phi K^*$ modes use seven variables: $K^+\pi^-$ candidate mass ($m_{K\pi}$), and K^* candidate's cosine of the helicity angle ($\cos\theta_{H,K^*}$) in addition to the ones used in $B \to \phi K$ modes. By fitting data, we determine the following quantities:

- Branching fractions: $\mathscr{B} = \frac{N}{\varepsilon\times 2\times N_{BB}}$, where N is the signal yield, ε is the signal reconstruction efficiency determined from simulation and validated with control samples, and N_{BB} is the number of $B\overline{B}$ events (19.7M for B^+B^- and 18.7M for $B^0\overline{B}^0$). N_{BB} is obtained from the measured integrated luminosity, the exclusive $e^+e^- \to \Upsilon(4S)$ cross section, and $\mathscr{B}(\Upsilon(4S) \to B^0\overline{B}^0)$ [10].

- CP asymmetries: The raw asymmetries are obtained by $\mathscr{A} = \frac{N(b)-N(\overline{b})}{N(b)+N(\overline{b})}$, where $N(b)$ and $N(\overline{b})$ are the yields of the final state with b and $\overline{b}$ flavors, respectively. The CP asymmetry is obtained by considering the instrumental effect: $\mathscr{A} = \mathscr{A}_{CP} + \mathscr{A}_{det}$. $\mathscr{A}_{det}(K^+\pi^-) = -0.010 \pm 0.003$ and $\mathscr{A}_{det}(K^0_S\pi^+) = -0.010 \pm 0.003$ are measured by using large samples of $D^0 \to K^+\pi^-$ and $D^+ \to K^0_S\pi^+$ decays with negligible CP violation. Then, $\mathscr{A}_{det}(K^+) = -0.015 \pm 0.022$ is obtained from $\mathscr{A}_{det}(K^+) = \mathscr{A}_{det}(K^+\pi^-) - \mathscr{A}_{det}(K^0_S\pi^+) + \mathscr{A}_{det}(K^0_S)$ [11].

- Longitudinal polarization fractions: $f_L = \frac{N_L/\varepsilon_L}{N_L/\varepsilon_L + N_T/\varepsilon_T}$, where $N_{L(T)}$ and $\varepsilon_{L(T)}$ is the signal yield and signal reconstruction efficiency with longitudinal (transverse) polarization, respectively. The distinctive helicity angle distributions allow for separating the two signal components.

Figures 1–8 show the ΔE distributions in data for $B^0 \to K^+\pi^-$, $B^0 \to \pi^+\pi^-$, $B^+ \to K^+\pi^0$, $B^+ \to \pi^+\pi^0$, $B^+ \to K^0\pi^+$, $B^0 \to K^0\pi^0$, $B^+ \to K^+K^-K^+$, and $B^+ \to K^+\pi^-\pi^+$ decays, with fit projection overlaid. Figure 9 shows the ΔE, $M_{\rm bc}$, C'_{out}, $m_{K^+K^-}$, and $\cos\theta_{H,\phi}$ distributions in data for $B^+ \to \phi K^+$ and $B^0 \to \phi K^0$ decays, with fit projections overlaid. Figure 10 shows the ΔE, $M_{\rm bc}$, C'_{out}, $m_{K^+K^-}$, $\cos\theta_{H,\phi}$, $m_{K\pi}$, and $\cos\theta_{H,K^*}$ distributions in data for $B^+ \to \phi K^{*+}$ and $B^0 \to \phi K^{*0}$ decays, with fit projections overlaid. The major systematic uncertainties come from tracking, PID, and fit modelling. All the measurement results are summarized in Table 1.

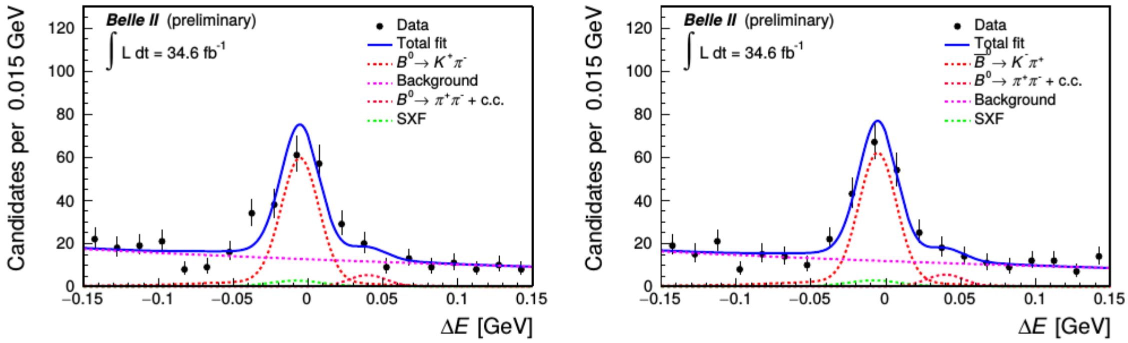

Figure 1: Distribution of ΔE for $B^0 \to K^+\pi^-$ (left) and $\overline{B}^0 \to K^-\pi^+$ (right) decays with fit projections overlaid.

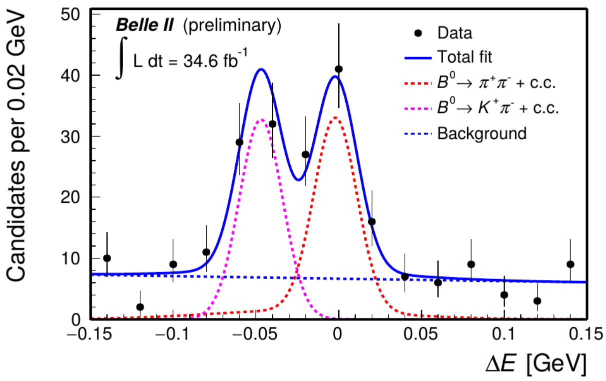

Figure 2: Distribution of ΔE for $B^0 \to \pi^+\pi^-$ decays with fit projections overlaid.

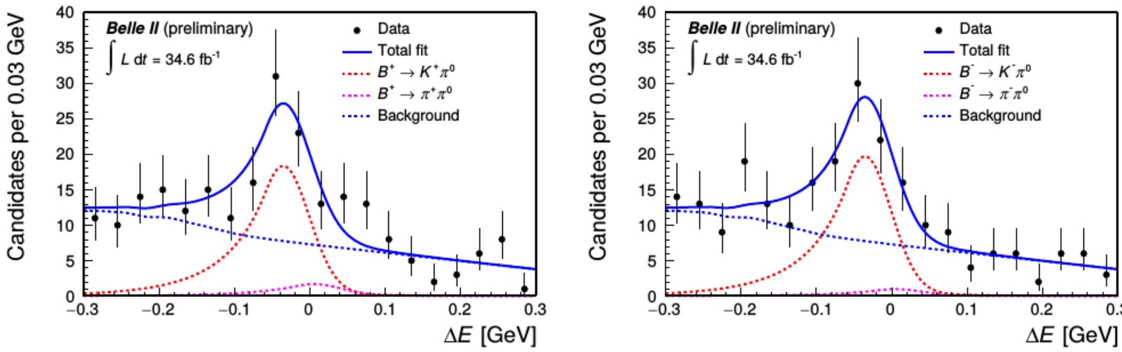

Figure 3: Distribution of ΔE for $B^+ \to K^+\pi^0$ (left) and $B^- \to K^-\pi^0$ (right) decays with fit projections overlaid.

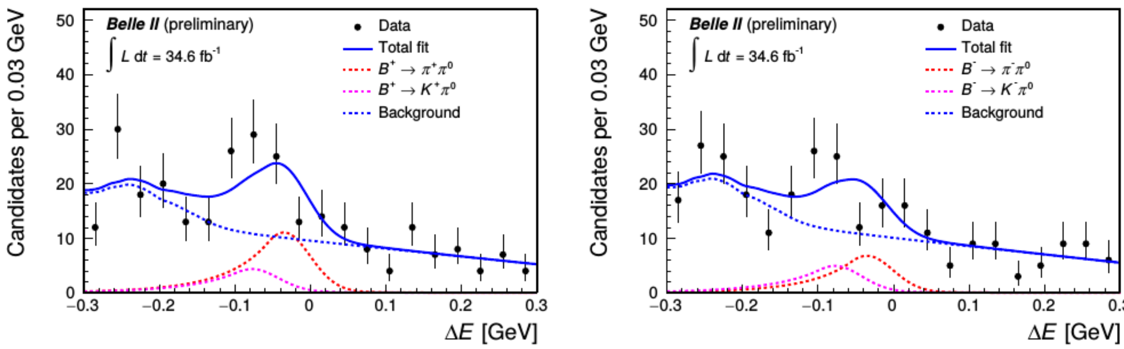

Figure 4: Distribution of ΔE for $B^+ \to \pi^+\pi^0$ (left) and $B^+ \to \pi^-\pi^0$ (right) decays with fit projections overlaid.

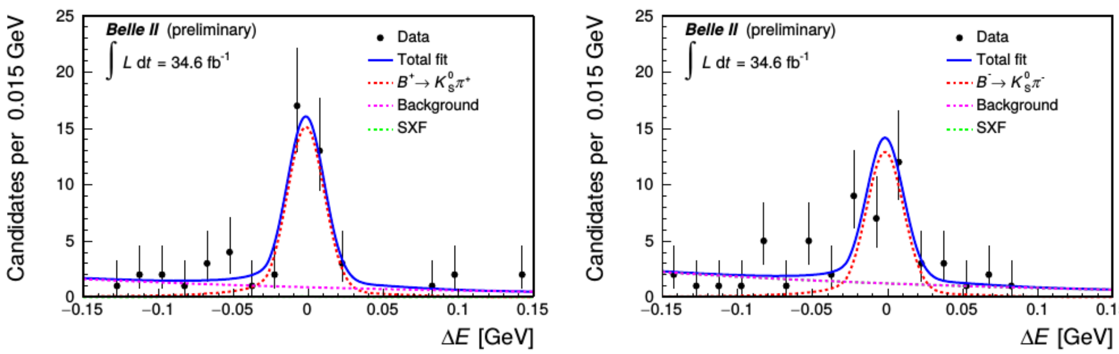

Figure 5: Distribution of ΔE for $B^+ \to K^0_S\pi^+$ (left) and $B^- \to K^0_S\pi^-$ (right) decays with fit projections overlaid.

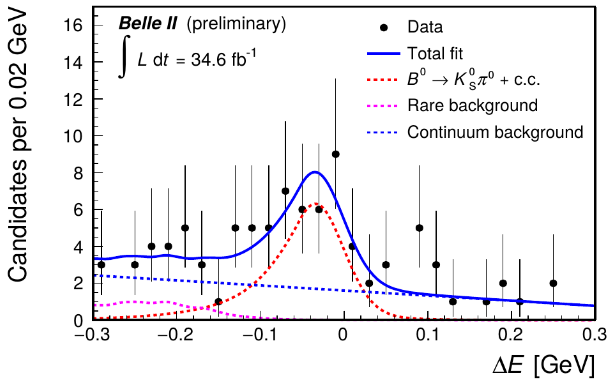

Figure 6: Distribution of ΔE for $B^0 \to K_S^0\pi^0$ decays with fit projections overlaid.

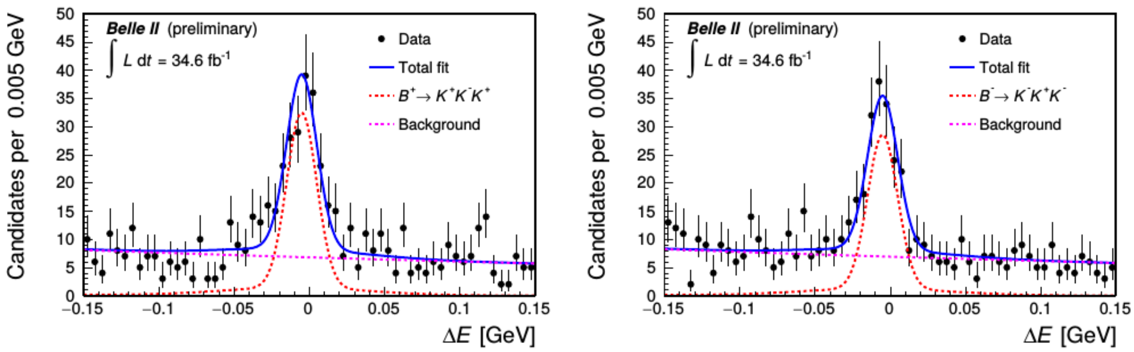

Figure 7: Distribution of ΔE for $B^+ \to K^+K^-K^+$ (left) and $B^- \to K^-K^+K^-$ (right) decays with fit projections overlaid.

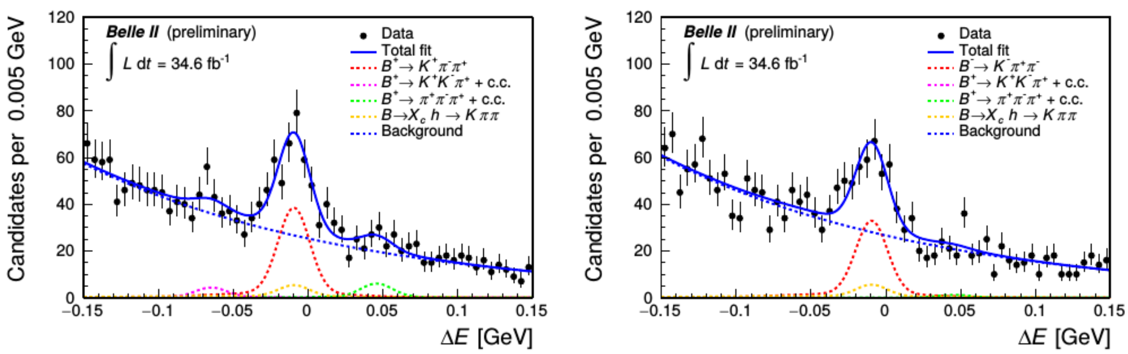

Figure 8: Distribution of ΔE for $B^+ \to K^+\pi^-\pi^+$ (left) and $B^- \to K^-\pi^+\pi^-$ (right) decays with fit projections overlaid.

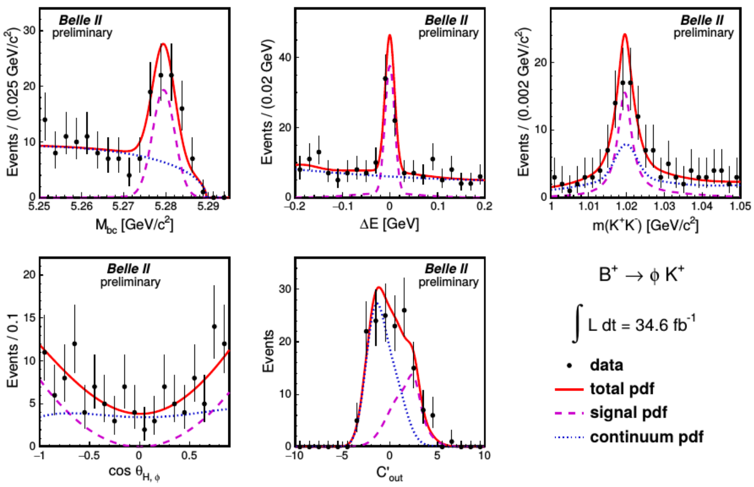

(a) $B^+ \to \phi K^+$

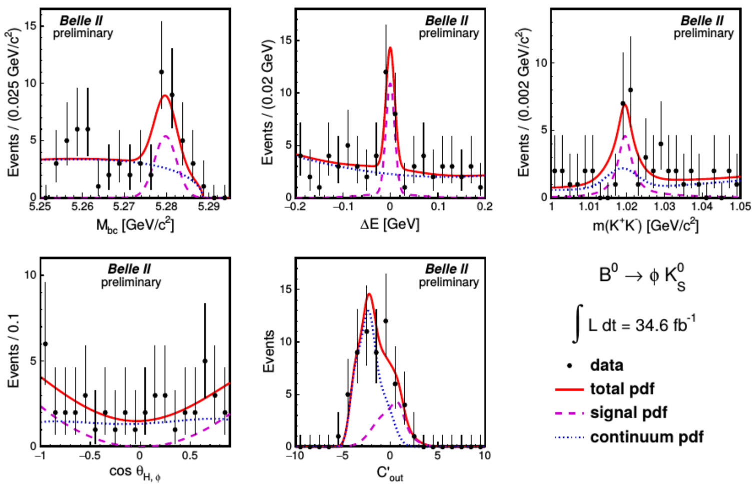

(b) $B^0 \to \phi K^0$

Figure 9: Distribution of ΔE, $M_{\rm bc}$, C'_{out}, $m_{K^+K^-}$, and $\cos\theta_{H,\phi}$ for $B^+ \to \phi K^+$ and $B^0 \to \phi K^0$ decays with fit projections overlaid.

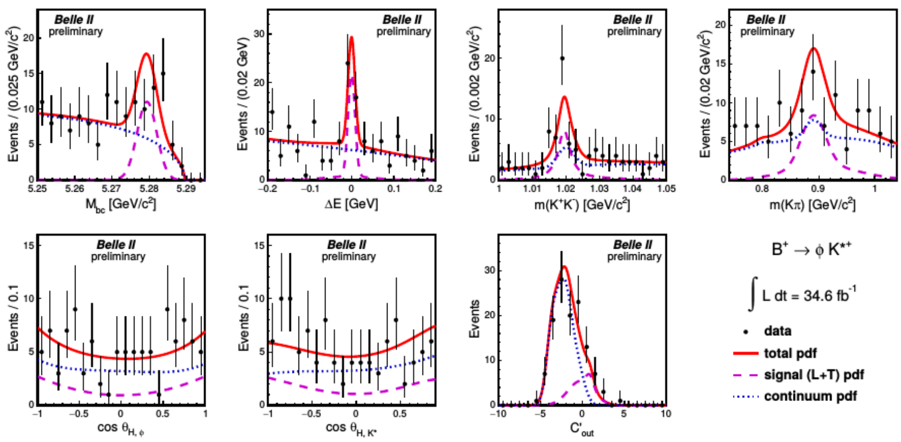

(a) $B^+ \to \phi K^{*+}$

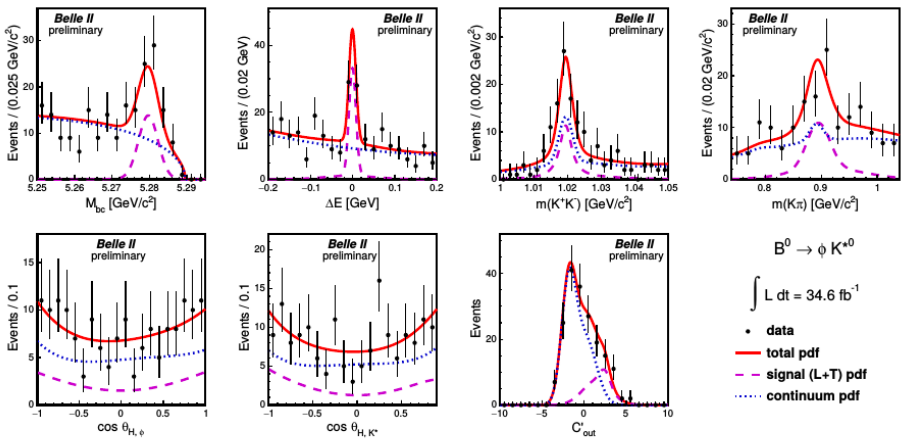

(b) $B^0 \to \phi K^{*0}$

Figure 10: Distribution of ΔE, $M_{\rm bc}$, C'_{out}, $m_{K^+K^-}$, $\cos\theta_{H,\phi}$, $m_{K\pi}$, and $\cos\theta_{H,K^*}$ for $B^+ \to \phi K^{*+}$ and $B^0 \to \phi K^{*0}$ decays with fit projections overlaid.

Table 1: Summary of measurement results. The first uncertainties in the values are statistical and the second ones are systematic.

Mode	$\mathscr{B}$ (10^{-6})	$\mathscr{A}_{CP}$	f_L
$B^0 \to K^+\pi^-$	$18.9 \pm 1.4 \pm 1.0$	$0.030 \pm 0.064 \pm 0.008$	-
$B^0 \to \pi^+\pi^-$	$5.6^{+1.0}_{-0.9} \pm 0.3$	-	-
$B^+ \to K^+\pi^0$	$12.7^{+2.2}_{-2.1} \pm 1.1$	$0.052^{+0.121}_{-0.119} \pm 0.022$	-
$B^+ \to \pi^+\pi^0$	$5.7 \pm 2.3 \pm 0.5$	$-0.268^{+0.249}_{-0.322} \pm 0.123$	-
$B^+ \to K^0\pi^+$	$21.8^{+3.3}_{-3.0} \pm 2.9$	$-0.072^{+0.109}_{-0.114} \pm 0.024$	-
$B^0 \to K^0\pi^0$	$10.9^{+2.9}_{-2.6} \pm 1.6$	-	-
$B^+ \to K^+K^-K^+$	$32.0 \pm 2.2 \pm 1.4$	$-0.049 \pm 0.063 \pm 0.022$	-
$B^+ \to K^+\pi^-\pi^+$	$48.0 \pm 3.8 \pm 3.3$	$-0.063 \pm 0.081 \pm 0.023$	-
$B^0 \to \phi K^0$	$5.9 \pm 1.8 \pm 0.7$	-	-
$B^+ \to \phi K^+$	$6.7 \pm 1.1 \pm 0.5$	-	-
$B^0 \to \phi K^{*0}$	$11.0 \pm 2.1 \pm 1.1$	-	$0.57 \pm 0.20 \pm 0.04$
$B^{*+} \to \phi K^{*+}$	$21.7 \pm 4.6 \pm 1.9$	-	$0.58 \pm 0.23 \pm 0.02$

4. Summary

Belle II reports first measurements in charmless B decays with a data sample corresponding to 34.6 fb^{-1}. The measurements include branching fractions, CP asymmetries, and longitudinal polarization fractions. All the results are in agreement with the known values, and offer good validations on the detector performance and analysis strategies.

References

[1] E. Kou *et al.* (Belle II Collaboration), PTEP **2019** (2019) no.12, 123C01, arXiv:1808.10567 [hep-ex].

[2] M. Gronau and D. London, Phys. Rev. Lett. **65** (1990) 3381 .

[3] M. Gronau, Phys. Lett. B **627** (2005) no. 1, 82-88.

[4] A. L. Kagan, Phys. Lett. B **601** (2004) no. 3 151-163.

[5] M. Beneke, J. Rohrer, and D. Yang, Phys. Rev. Lett. **96** (2006) 141801.

[6] K. Akai *et al.*, Nucl. Instrum. Meth. A **907** (2018) 188-199 .

[7] T. Abe *et al.* (Belle II Collaboration), arXiv:1011.0352 [hep-ex].

[8] F. Abudinén (Belle II Collaboration), arXiv:2009.09452 [hep-ex].

[9] F. Abudinén (Belle II Collaboration), arXiv:2008.03873 [hep-ex].

[10] A. J. Bevan *et al.* (Belle and BaBar Collaborations), Eur. Phys. J. **C74** (2014) 3026, arXiv:1406.6311 [hep-ex].

[11] A. Davis *et al.* (LHCb Collaboration), [LHCb-PUB-2018-004].